Real-Time Temperature Reconstruction in Microwave Hyperthermia: ESHO Models Validation

# Real-Time Temperature Reconstruction in Microwave Hyperthermia: ESHO Models Validation

Maryam Firuzalizadeh[1], Rossella Gaffoglio[2], Giorgio Giordanengo[2], Marco Righero[2], and Giuseppe Vecchi[1]
[1]Department of Electronics and Telecommunications, Politecnico di Torino, Torino, Italy, maryam.firuzalizadeh@polito.it
[2]Advanced Computing, Photonics & Electromagnetics, Fondazione LINKS, Torino, Italy

***Abstract*—Accurate temperature monitoring remains a challenge in microwave hyperthermia (HT), in particular for deep-seated tumors. Recent work has demonstrated that combining scarce temperature measurements with precomputed simulation libraries enables real-time 3D temperature reconstruction in the entire region of interest (ROI). In this study, we validate this reconstruction strategy using the standardized benchmark models released by the European Society for Hyperthermic Oncology (ESHO), strictly following all ESHO guidelines for numerical simulation and verification in hyperthermia treatment planning (HTP). Results obtained with the "Alex" head and neck benchmark model confirm the possibility to achieve an average error lower than 0.4 °C in 95% of the ROI even when the sensor points used in the reconstruction are scarce and affected by noise.**

***Index Terms*—Microwave hyperthermia (HT), European Society for Hyperthermic Oncology (ESHO) benchmarks, hyperthermia treatment planning (HTP), invasive thermometry, temperature reconstruction.**

## I. Introduction

Microwave hyperthermia (HT) is a clinically well-established adjuvant cancer therapy that enhances the effectiveness of radiotherapy and chemotherapy by increasing tumor temperatures to 40–44°C [1]. Achieving effective yet safe heating requires accurate control of the spatial temperature distribution: insufficient heating of tumor tissue compromises efficacy, while overheating of healthy tissues can cause irreversible damage. Reliable temperature monitoring is therefore critical for both safety and effectiveness in hyperthermia treatments.

In current clinical practice, temperature monitoring is limited to invasive thermometry, usually performed via catheters, that provide information only at a few discrete points [2]. Causing discomfort to the patient, the number of catheters must be reduced to the bare minimum, thus preventing a comprehensive assessment of the temperature distribution within the region of interest (ROI). Alternative non-invasive techniques for temperature monitoring, such as magnetic resonance thermometry, are currently under development [3], but still suffer from motion sensitivity and susceptibility artifacts, and remain impractical in many treatment scenarios due to cost and logistical constraints.

A recently proposed approach addresses the current absence of a real-time precise technique for 3D temperature monitoring by combining scarse temperature measurements with a library of pre-computed simulated temperature maps [4]. The goal of this technique is to create a patient-specific library of multiphysics simulations before treatment, which accounts for uncertainties in tissue properties. During treatment, scarce temperature data from minimally invasive catheters, which can also be intraluminal (non-invasive), are used to match the simulations, effectively reducing uncertainty and providing a reliable 3D temperature map of the ROI in real time.

The European Society for Hyperthermic Oncology (ESHO) has published benchmark models [5] that define geometries, dielectric and thermal parameters, and evaluation standards to ensure reproducibility and comparability of numerical methods. In this work, we validate the reconstruction approach proposed in [4] using the ESHO benchmark model "Alex", fully following the ESHO guidelines. This validation has the goal to further assess the reconstruction method within the HT community and to demonstrate compliance with the established standards.

## II. Method

The reconstruction algorithm follows the workflow introduced in [4], here adapted and validated on the ESHO benchmark model [5]. The goal is to reconstruct the spatial temperature distribution within the region of interest (ROI) from a limited number of measurements. The temperature field is evaluated using the steady-state Pennes' bioheat equation [6], solved under appropriate boundary conditions as defined by the ESHO guidelines [5].

A set of $B$ steady-state temperature maps is generated using the Sim4Life platform [7], each obtained by varying the thermal parameters of the most relevant tissues within realistic uncertainty ranges according to a low-discrepancy Sobol sequence. These simulations, referred to as reconstruction maps, $\phi_b(\boldsymbol{r})$, $b = 1, ..., B$, represent the steady-state temperature distributions corresponding to different parameter combinations ($\boldsymbol{s}_b$) extracted using a Sobol sequence.

To simulate the treatment condition, we consider only a limited number of noisy temperature measurements $\tilde{T}(\boldsymbol{q}_\ell)$, $\ell = 1, \ldots, L$, available at known locations $\boldsymbol{q}_\ell$ along the inserted catheter. These points represent the "known" temperature measurements used during reconstruction, whereas the full temperature field is unknown (i.e., the target temperature map $T(\boldsymbol{r})$). Since measurement points are inherently affected by noise, a Gaussian noise was added to the known temperature values to simulate the uncertainty introduced by the

temperature sensing system. The noisy temperature samples were modeled as:

$$\tilde{T}(\boldsymbol{q}_\ell) = T(\boldsymbol{q}_\ell) + f_{\mathcal{N}}(\boldsymbol{q}_\ell; \mu, \sigma^2), \tag{1}$$

here, $f_{\mathcal{N}}$ is a function generating an array of random errors, normally distributed with mean $\mu$ and variance $\sigma^2$.

The overall temperature distribution in the ROI is then reconstructed as a combination of the precomputed maps:

$$\hat{T}(\boldsymbol{r}) = \sum_{b=1}^{B} w_b \, \phi_b(\boldsymbol{r}), \tag{2}$$

where $w_b$ are the corresponding weights. The optimal coefficients $w_b$ are determined by solving a constrained least-squares (CLS) problem that minimizes the discrepancy between simulated and measured data, i.e.:

$$\min_{\boldsymbol{w}\in\mathbb{R}^B} \sum_{\ell=1}^{L} \left( \sum_{b=1}^{B} w_b \, \phi_b(\boldsymbol{q}_\ell) - \tilde{T}(\boldsymbol{q}_\ell) \right)^2, \tag{3}$$

subject to the additional constraints:

$$\sum_{b=1}^{B} w_b = 1, \quad \text{and} \quad w_b \geq 0, \quad \forall b = 1, \ldots, B. \tag{4}$$

The resulting reconstructed map $\hat{T}(\boldsymbol{r})$ provides a robust estimate of the steady-state temperature distribution even when only scarce, noisy measurements are available.

Following the definition introduced in [4], a goodness function $g(\chi)$ is employed to quantify the reconstruction accuracy. This metric measures the fraction of the ROI where the absolute temperature error remains below a threshold $\chi$:

$$g(\chi) = \frac{\mathrm{Vol}(\{\boldsymbol{r} \in \mathrm{ROI} : \Delta T \leq \chi\})}{\mathrm{Vol}(\mathrm{ROI})}, \tag{5}$$

where $\Delta T$ represents the absolute temperature difference between the reconstructed temperature map $\hat{T}(\boldsymbol{r})$ and the target temperature map (i.e., the simulated ground-truth temperature map $T(\boldsymbol{r})$, which was not included in the reconstruction database).

## III. Verification on ESHO Model

Numerical simulations were performed using the ESHO "Alex" head-and-neck (H&N) model implemented in the Sim4Life platform [7], which provides standardized geometry, the antenna applicator, electromagnetic (EM) and thermal modeling, and material assignments [5].

Figure 1a illustrates the Alex model with the benchmark H&N applicator, consisting of twelve half-wavelength dipole antennas distributed over three rings. Figure 1b shows the top view of the horse-shoe applicator and the clinically used waterbolus. The gross tumor volume (GTV) located in the nasopharyngeal region is shown in Fig. 2, where only bones and tumor are visualized for clarity.

Electromagnetic fields were computed using a finite-difference time-domain (FDTD) solver provided by Sim4Life [7]. The amplitude and phase coefficients of the array were optimized using a Specific Absorption Rate (SAR)-based procedure to maximize power deposition within the tumor while minimizing the risk of overheating in the surrounding healthy tissues [8]. SAR-based optimizations are commonly used in the clinical practice, offering a good trade-off between computational demand and heating accuracy [9], [10]. The resulting optimized excitations with an input power of 290 W yield a sufficiently good SAR pattern around the tumor, similar to that reported in the ESHO guidelines [5] (see Fig. 3).

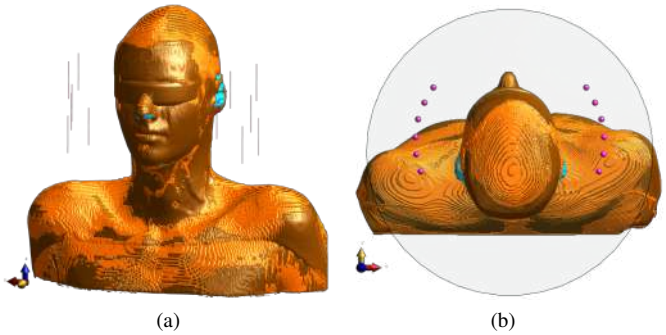

(a) (b)

Fig. 1. (a) Visualization of the ESHO "Alex" H&N patient model with the benchmark H&N applicator consisting of twelve half-wavelength dipole antennas distributed over three rings; (b) top view of the Alex model with the horse-shoe applicator and the considered waterbolus.

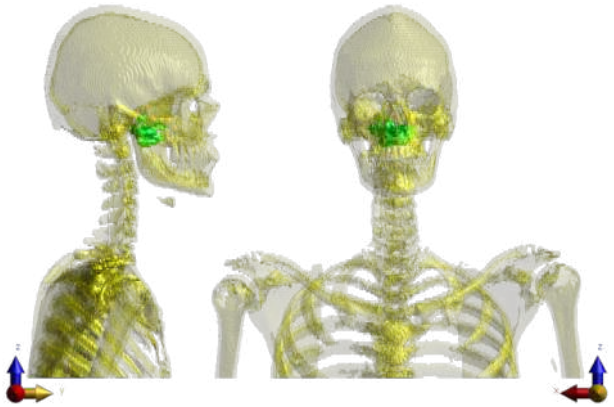

Fig. 2. Gross tumor volume (GTV) in the nasopharyngeal region of the Alex model. Only the bones and the tumor are shown for clarity.

In the Alex model, a preliminary analysis was carried out to identify the most relevant tissues within the ROI, which were found to be muscle, fat, cerebrum, and tumor.

The ranges of variation reported in Table I were employed to generate the ensemble of simulated temperature maps $\phi_b(\boldsymbol{r})$ forming the reconstruction basis. All remaining tissue parameters were set to their baseline values reported in the ESHO database [5].

Using $B = 70$ reconstruction maps, the $g(\chi)$ indicator defined in Eq. 5 has been estimated for two catheter configurations and shown in Fig. 4. In the first example (Catheter Case 1) $L = 20$ temperature sensor points distributed along the nasal cavity were considered, representing a non-invasive (in-

TABLE I
Considered tissues' properties, baseline values, and range of variation

| | $k$ (W/m°C) | | | $\omega$ (ml/(min kg)) | | |
|---|---|---|---|---|---|---|
| Tissue | Baseline | min | max | Baseline | min | max |
| Muscle | 0.49 | 0.40[a] | 0.56[a] | 188.7 | 19[a] | 442.8[a] |
| Fat | 0.21 | 0.18[a] | 0.50[a] | 69 | 20[a] | 255[a] |
| Cerebrum | 0.55 | 0.53[b] | 0.56[b] | 763.3 | 671[b] | 840[b] |
| Tumor | 0.49 | 0.41[a] | 1.50[a] | 94.4 | 36.15[a] | 848[a] |

The baseline values are derived from the ESHO benchmarck database [5]. **a**: values as used in [4]; **b**: values derived from the IT'IS database [11].

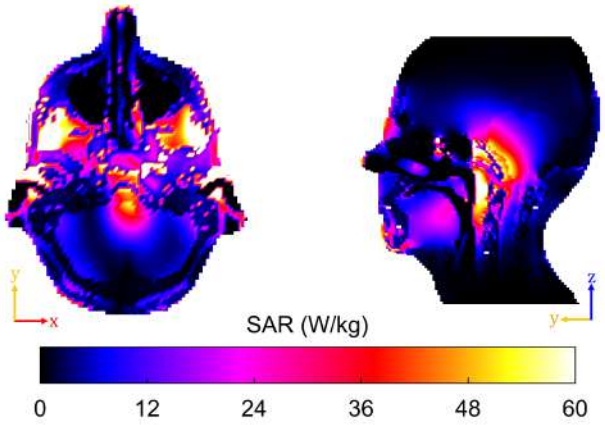


Fig. 3. Axial and sagittal cross-sections of the optimized SAR distribution in the ESHO model Alex.

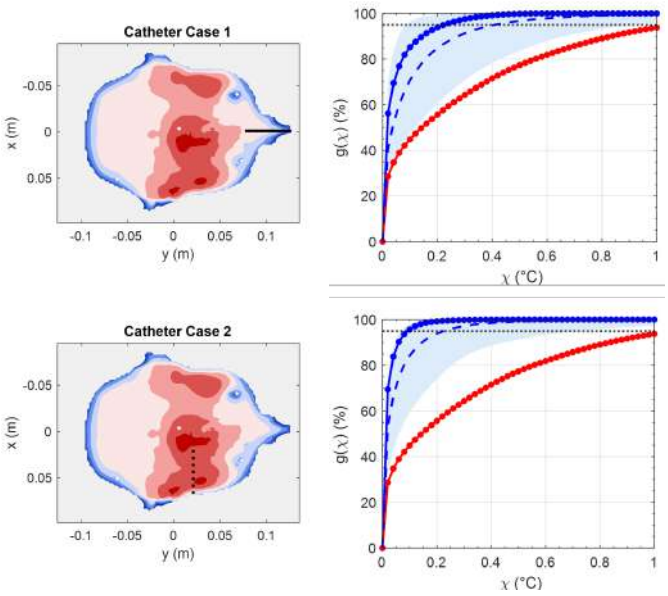


(a) (b)

Fig. 4. Reconstruction performance for two catheter configurations. (a) Measurement point locations (black dots) overlaid on the baseline temperature map for Catheter Case 1 ($L = 20$ points along the nasal path, non-invasive) and Catheter Case 2 ($L = 7$ invasive points). (b) Corresponding $g(\chi)$ curves comparing reconstructed and target temperature maps. The blue-dot line corresponds to the reconstruction of the target map without noise, the blue-shadow region includes 2000 realizations of the Gaussian error ($\mu = \pm 0.1$°C and $\sigma = 0.2$°C), with the blue dashed line denoting the average; the red-dot line expresses the discrepancy between the target map and the baseline map.

traluminal) thermometry setup. The second example (Catheter Case 2) employed an invasive configuration with only $L = 7$ probes to evaluate the method's robustness under limited spatial sampling. Fig. 4a shows the sensors position overlaid on the baseline temperature distribution (i.e. the temperature map extracted using the baseline parameters of Table I), while Fig. 4b illustrates the corresponding goodness functions $g(\chi)$.

The blue-dotted curve in Fig. 4b represents the ideal (noise-free) reconstruction. The shaded blue region depicts 2000 realizations of Gaussian noise ($\mu = \pm 0.1$°C, $\sigma = 0.2$°C), while the dashed blue line shows their mean performance. Even in the presence of noise on the scarce measurement points, the reconstructed temperature fields achieve an average error lower than 0.4 °C in 95% of the ROI, confirming the robustness of the approach. The red-dotted curve expresses the discrepancy between the baseline and target maps, serving as a reference for assessing reconstruction quality.

These results, obtained using the ESHO "Alex" benchmark model, confirm that accurate 3D temperature reconstructions can be achieved even under scarce and noisy measurement conditions, based on the approach proposed in [4].

## IV. Conclusion

This study validates a real-time temperature reconstruction method on the standardized ESHO "Alex" head-and-neck model, ensuring full compliance with benchmark modeling guidelines.

The core of the proposed framework lies in two main steps: (1) the creation of a pre-treatment library of multiphysics simulations obtained by varying the relevant tissue parameters within realistic uncertainty ranges, and (2) the real-time reconstruction of the temperature maps from a limited number of noisy measurements acquired during treatment. By selecting and combining the precomputed simulations that best match the scarce temperature data, the method effectively reduces model uncertainty and provides reliable estimates of the full 3D temperature distribution within the ROI.

Validation on the ESHO "Alex" benchmark model demonstrates that an average error lower than 0.2 °C in 95% of the ROI can be achieved even when relying on a limited number of scarce and noisy invasive measurements. Furthermore, the reconstruction performance obtained in the non-invasive nasal configuration (average error $< 0.4$°C in 95% of the ROI) confirms that accurate temperature monitoring can be achieved without any invasive probing, highlighting the robustness and flexibility of the approach. The technique therefore represents a promising step toward minimally invasive, real-time thermometry and adaptive control in clinical hyperthermia treatments.

Future developments will focus on extending the framework to a more exhaustive set of target maps and catheter configurations as well as considering transient heating conditions. Detailed quantitative results and uncertainty analyses will be

presented at the Conference.

## ACKNOWLEDGMENT

The authors acknowledge ZMT Zurich MedTech for providing access to the *Sim4Life* software under a research license agreement. The authors also would like to thank Kemal Sumser for providing the ESHO model of Alex and the associated dataset.

## REFERENCES

[1] N. R. Datta *et al.*, "Local hyperthermia combined with radiotherapy and-/or chemotherapy: Recent advances and promises for the future," *Cancer Treat. Rev.*, vol. 41, no. 9, pp. 742–53, 2015.

[2] H. P. Kok and J. Crezee, "Hyperthermia treatment planning: Clinical application and ongoing developments," *IEEE Journal of Electromagnetics, RF and Microwaves in Medicine and Biology*, vol. 5, no. 3, pp. 214–222, 2021.

[3] G. C. van Rhoon and P. W. and, "Introduction: Non-invasive thermometry for thermotherapy," *International Journal of Hyperthermia*, vol. 21, no. 6, pp. 489–495, 2005.

[4] R. Gaffoglio, G. Giordanengo, M. Righero, M. Zucchi, M. Firuzalizadeh, G. Musacchio Adorisio, A. Bellone, A. Vallan, G. Perrone, and G. Vecchi, "Real-time 3D temperature reconstruction in microwave cancer hyperthermia from scarce temperature measurements," *Nat. Commun.*, vol. 16, no. 1, p. 4824, 2025.

[5] M. M. Paulides *et al.*, "ESHO benchmarks for computational modeling and optimization in hyperthermia therapy," *Int. J. Hyperthermia*, vol. 38, no. 1, pp. 1425–1442, 2021.

[6] H. H. Pennes, "Analysis of tissue and arterial blood temperatures in the resting human forearm," *J Appl Physiol*, vol. 1, no. 2, pp. 93–122, 1948.

[7] Sim4Life, *version 7.0.2.10006*. https://zmt.swiss/sim4life/, 2022.

[8] M. Firuzalizadeh, R. Gaffoglio, G. Giordanengo, M. Righero, M. Zucchi, G. Musacchio Adorisio, A. Bellone, A. Vallan, G. Perrone, and G. Vecchi, "Joint Optimization of Antenna System Matching and Specific Absorption Rate Focusing in Microwave Hyperthermia Cancer Treatment," *Cancers*, vol. 17, no. 3, 2025.

[9] Z. Rijnen *et al.*, "Clinical integration of software tool VEDO for adaptive and quantitative application of phased array hyperthermia in the head and neck," *Int. J. Hyperthermia*, vol. 29, no. 3, pp. 181–93, 2013.

[10] R. Gaffoglio, M. Righero, G. Giordanengo, M. Zucchi, and G. Vecchi, "Fast Optimization of Temperature Focusing in Hyperthermia Treatment of Sub-Superficial Tumors," *IEEE J. Electromagn. RF Microw. Med. Biol.*, vol. 5, no. 3, pp. 286–293, 2021. [Online]. Available: https://ieeexplore.ieee.org/document/9290118/

[11] P. A. Hasgall *et al.*, *IT'IS database for thermal and electromagnetic parameters of biological tissues*. IT'IS Foundation, 2018. [Online]. Available: http://www.itis.ethz.ch/database